Report

Current Biology

Kinematic Diversity in Rorqual Whale Feeding Mechanisms

Graphical Abstract

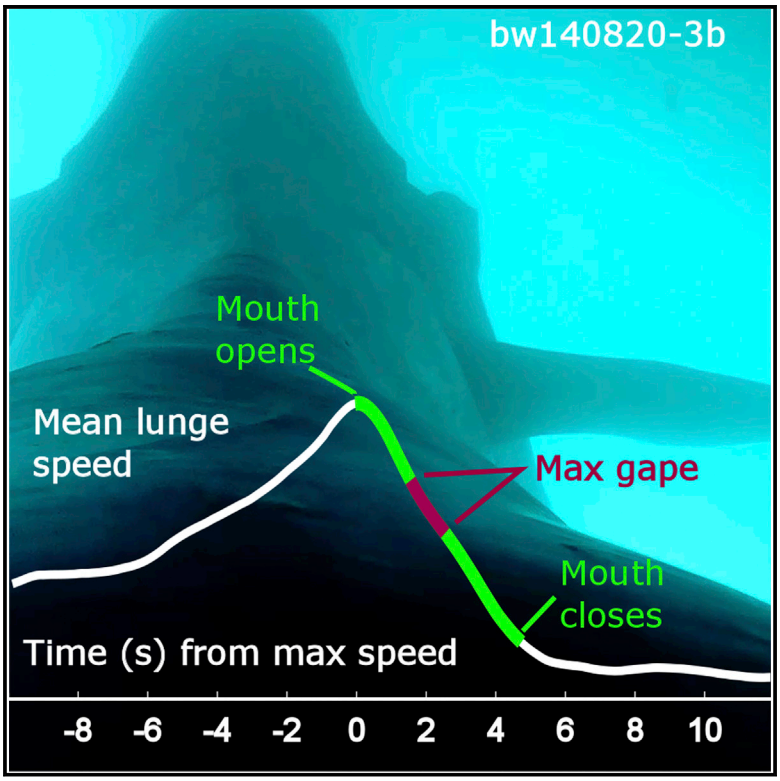

Highlights

- Tags with both video and 3D accelerometry were deployed on feeding rorquals
- Skull movement could be observed in concert with animal orientation and motion
- Lunging whales displayed prey-dependent inter- and intra-species kinematic diversity
- Humpback whales most likely sacrifice energy efficiency to increase foraging flexibility

Authors

David E. Cade, Ari S. Friedlaender, John Calambokidis, Jeremy A. Goldbogen

Correspondence

davecade@stanford.edu

In Brief

Rorqual lunge feeding has been assumed to be kinematically similar across species. Cade et al. use new video and accelerometry tags to show that blue whales, krill specialists, and humpback whales, foraging generalists, have similarly stereotypical lunges on krill—but humpbacks feeding on fish demonstrate kinematic diversity in lunge timing.

Cade et al., 2016, Current Biology *26*, 1–8
October 10, 2016
http://dx.doi.org/10.1016/j.cub.2016.07.037

CellPress

Please cite this article in press as: Cade et al., Kinematic Diversity in Rorqual Whale Feeding Mechanisms, Current Biology (2016), http://dx.doi.org/10.1016/j.cub.2016.07.037

Current Biology
Report

Kinematic Diversity in Rorqual Whale Feeding Mechanisms

David E. Cade,[1,4,*] Ari S. Friedlaender,[2] John Calambokidis,[3] and Jeremy A. Goldbogen[1]
[1]Department of Biology, Hopkins Marine Station, Stanford University, Pacific Grove, CA 93950, USA
[2]Marine Mammal Institute, Hatfield Marine Science Center, Department of Fish and Wildlife, Oregon State University, Newport, OR 97365, USA
[3]Cascadia Research Collective, 218 1/2 West 4th Avenue, Olympia, WA 98501, USA
[4]Lead Contact
*Correspondence: davecade@stanford.edu
http://dx.doi.org/10.1016/j.cub.2016.07.037

SUMMARY

Rorqual whales exhibit an extreme lunge filter-feeding strategy characterized by acceleration to high speed and engulfment of a large volume of prey-laden water [1–4]. Although tagging studies have quantified the kinematics of lunge feeding, the timing of engulfment relative to body acceleration has been modeled conflictingly because it could never be directly measured [5–7]. The temporal coordination of these processes has a major impact on the hydrodynamics and energetics of this high-cost feeding strategy [5–9]. If engulfment and body acceleration are temporally distinct, the overall cost of this dynamic feeding event would be minimized. However, greater temporal overlap of these two phases would theoretically result in higher drag and greater energetic costs. To address this discrepancy, we used animal-borne synchronized video and 3D movement sensors to quantify the kinematics of both the skull and body during feeding events. Krill-feeding blue and humpback whales exhibited temporally distinct acceleration and engulfment phases, with humpback whales reaching maximum gape earlier than blue whales. In these whales, engulfment coincided largely with body deceleration; however, humpback whales pursuing more agile fish demonstrated highly variable coordination of skull and body kinematics in the context of complex prey-herding techniques. These data suggest that rorquals modulate the coordination of acceleration and engulfment to optimize foraging efficiency by minimizing locomotor costs and maximizing prey capture. Moreover, this newfound kinematic diversity observed among rorquals indicates that the energetic efficiency of foraging is driven both by the whale's engulfment capacity and the comparative locomotor capabilities of predator and prey.

RESULTS

Lunge feeding in rorqual whales (Balaenopteridae) is characterized by the rapid engulfment and subsequent filtration of large volumes—up to 160% of body mass [1]—of prey-laden water, but the precise mechanisms underlying this dynamic process remain poorly understood. The long-standing paradigm of lunge feeding consists of three discrete phases (Movies S1 and S2): (1) acceleration to high speed, (2) engulfment (Figures 1 and 2), and (3) filtration [5]. Lunge feeding at high speed generates dynamic pressure that is required to expand the ventral feeding pouch during engulfment [10, 11]. Quantification of the timing of the gape cycle relative to whale speed is critical for estimating the forces at play during lunge feeding and thus the energetic costs of foraging, yet to date this timing could only be assumed from indirect kinematic signatures [6–8, 12]. The kinematic signature of a rorqual lunge includes an increase in speed and overall body acceleration followed by a rapid deceleration [2, 7, 13, 14]. However, all prior studies either lacked direct observation of skull and jaw kinematics (e.g., [5–7]) or did not have kinematic sensors (e.g., [15]), and this led to conflicting hypotheses about the temporal relationship between the acceleration and engulfment phases: a peak speed mouth opening hypothesis [5, 6] and an early mouth opening hypothesis [7].

Using low-resolution (1 Hz) tag data from three rorqual species feeding on krill (Euphausiids) [2, 13, 14], Goldbogen et al. [5] and Potvin et al. [6] predicted that rorqual mouths open at maximum swim speed, followed by a discrete engulfment phase during deceleration. Hydrodynamic models of engulfment suggest that this decoupling of body acceleration and engulfment would increase the efficiency of lunge feeding with respect to prey capture but at a cost of increased drag from the acceleration of the water inside the mouth [6]. In contrast, higher-resolution (25 Hz) tag data from humpback whales feeding on an unknown prey type led Simon et al. [7] to the hypothesis that peaks in rate of acceleration (i.e., jerk) and minimum specific acceleration (MSA) during the acceleration phase implied higher than normal drag forces and thus that the mouth must open several seconds before maximum speed [7]. This hypothesis implied that rorquals continue accelerating during the mouth-opening phase, yielding a higher cost of transport during engulfment and a greater degree of forward momentum after mouth closure [7].

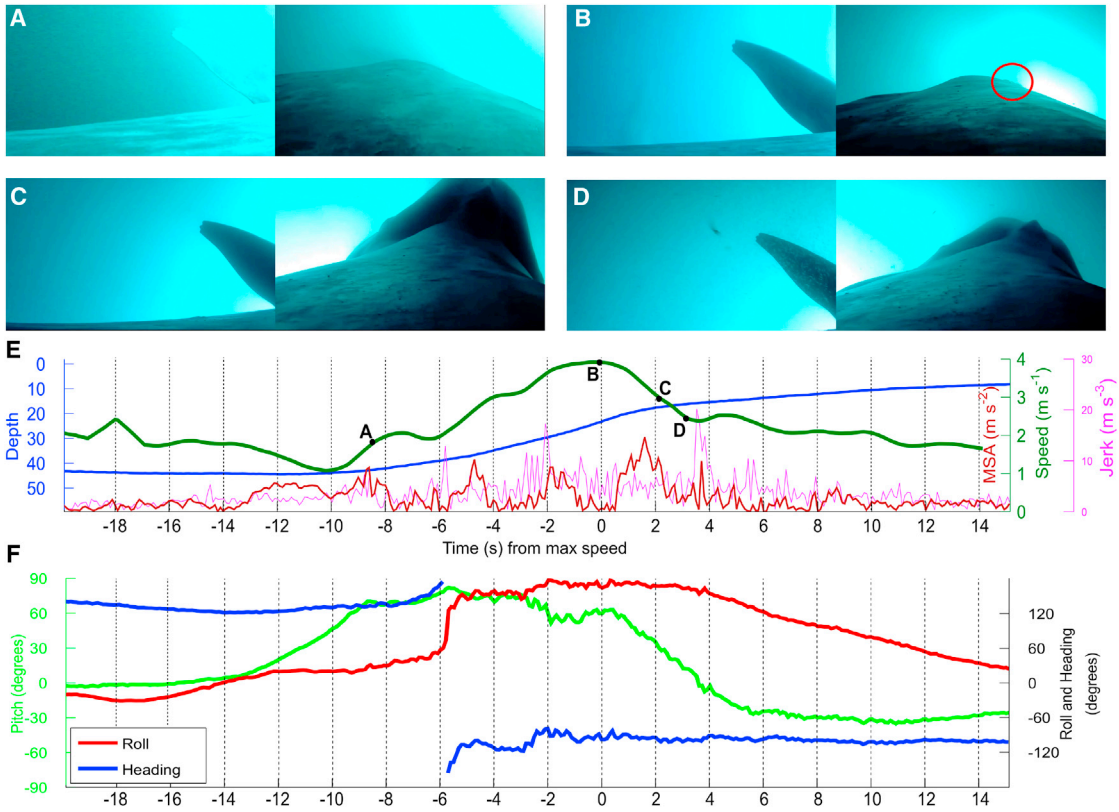

Figure 1. Visualization of a Blue Whale Feeding Event Using a CATS Tag that Integrates Dual, Forward-Facing Video Cameras with Orientation and Motion Sensors

(A) The whale is pitched upward at 70° at the start of the acceleration phase. The left flipper is visible in the left panel.

(B) At peak speed, the blow holes (homologous to the nostrils) are just visible above the back (red circle), signifying the start of upper-jaw lift.

(C) Maximum gape. At this moment, the whale is ventral side up, angled at a pitch of 32°.

(D) The upper jaw before complete mouth closure and before the animal spins to its left to return to normal position. The target prey (a krill swarm) can be seen in the left panel.

(E) Animal speed (derived from flow noise and smoothed with a 0.5 s running mean), depth, minimum specific acceleration (MSA), and jerk (calculated from 10 Hz accelerometry data). Letters correspond to the images above.

(F) Animal orientation described using the Euler angles pitch (green), roll (red), and heading (blue).

See Movie S1. This tag (bw140820-3b; Figure S1A; Table S1) was placed on the left side of the animal facing forward. Axis conventions are as in Figure S2.

To resolve this ambiguity, we developed a novel tag sensor suite including video cameras and high sample rate movement sensors (Figure S1; http://www.cats.is) that provide information on body kinematics not just at the location of tag attachment on the animal but also at points observable by the cameras, thus enabling measurements of how the engulfment phase overlaps with the acceleration phase in lunge-feeding rorquals. Data were obtained for krill-feeding blue whales (*Balaenoptera musculus*; six whales, 25 lunge-feeding events) off of California and Chile; krill-feeding humpback whales (*Megaptera novaeangliae*; four whales, 20 lunges) off of western South Africa and Monterey, CA; sand-lance-feeding humpback whales (three whales, 13 lunges) near Cape Cod, MA; and an anchovy-feeding humpback whale (one whale, 19 lunges) in Monterey Bay, CA.

Tag data and our kinematic analyses demonstrated that lunging blue whales opened their mouths 0.0 ± 1.0 s (mean ± SD) after peak speed, started closing their mouths 2.6 ± 1.3 s after peak speed, and had engulfment cycles totaling 4.9 ± 0.8 s (Table 1; Figures 1 and 3A). Krill-feeding humpback whales (Table 1; Figure 3B) had shorter engulfment cycles (2.0 ± 0.5 s) but similar timing in relation to peak speed (opening: 0.2 ± 0.7 s after peak; start closing: 1.3 ± 0.8 s after peak). Both groups closed their mouths very close to the inflection point when deceleration began to subside (Table 1; Figure 3), suggesting that peak speed and the inflection point may be good indicators of gape cycle for krill-feeding rorquals in the absence of video data. In contrast to the stereotypy exhibited by krill-feeding whales, humpback whales feeding on fish (Table 1; Figures 2 and 3C) had more variable engulfment durations (4.8 ± 3.0 s) and relationships of the engulfment cycle to speed (opening: 1.1 ± 2.8 s after peak; start closing: 4.4 ± 4.2 s after peak). When speed could be calculated from orientation-corrected depth rate (OCDR) [7], the timing of the peaks in speed was close to that for flow noise for all measured lunges (0.5 ± 0.5 s in absolute distance).

Our analyses were consistent with previous studies (e.g., [7, 16]) indicating higher MSA and jerk signals during lunge-feeding events compared to non-feeding swimming. Prior to

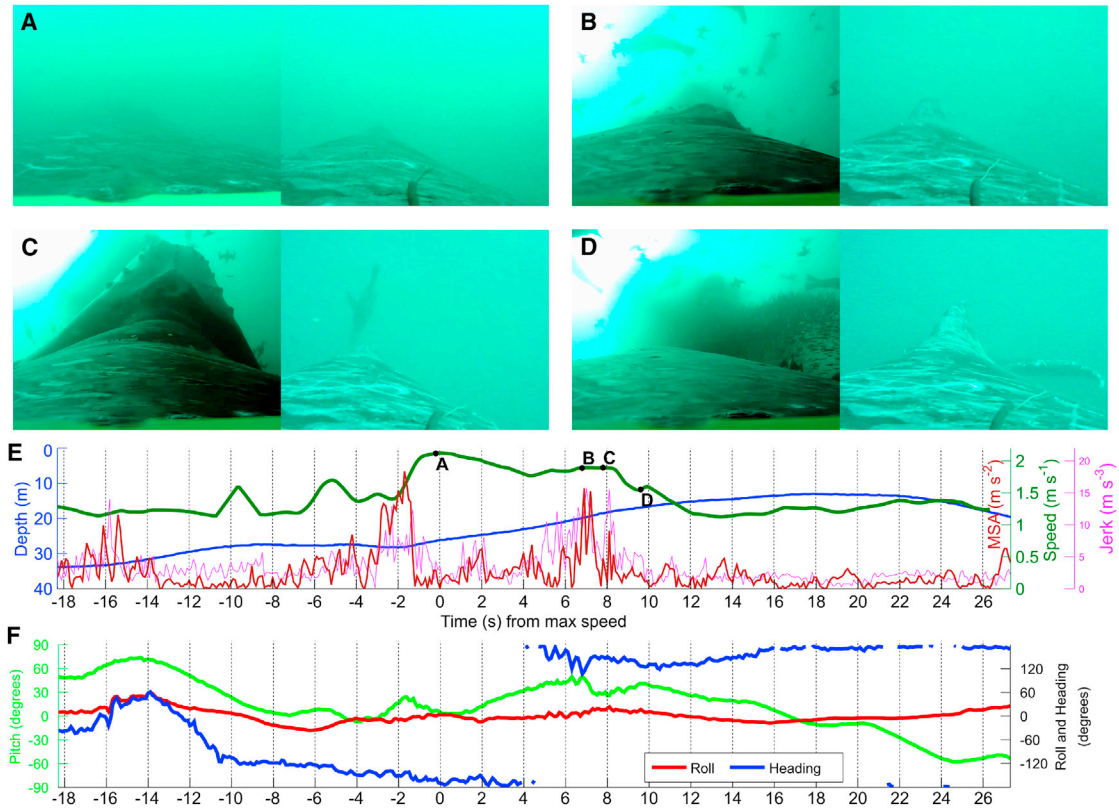

Figure 2. Visualization of a Humpback Whale Feeding on Anchovies

(A) At the peak in speed, the animal had not yet begun the lunge but was situated in a horizontal position 8 m below and to the left of a school of anchovies (*Engraulis mordax*).

(B) At a subsidiary peak, the mouth began to open with the whale pitched at 45° and moving to its right.

(C) Maximum gape directly before a steep deceleration.

(D) Evasive prey are seen attempting to avoid simultaneous predation by the tagged animal, Caliornia sea lions (*Zalophus californianus*), and diving sea birds.

(E) Animal speed (derived from flow noise and smoothed with a 0.5 s running mean), depth, MSA, and jerk (calculated from 10 Hz accelerometry data). Letters correspond to the images above.

(F) Animal orientation described using the Euler angles pitch (green), roll (red) and heading (blue).

See Movie S2. This tag (mn151012-7; Figure S1B; Table S1) was placed along the dorsal midline and had forward-facing (left) and rear-facing (right) cameras. Axis conventions are as in Figure S2.

confirmation with video, the peaks in jerk and MSA were suggested in the early mouth opening hypothesis to, respectively, be related to skull movement and indicative of working against maximum resistance from water entering the mouth [7]. However, we found that peaks in both MSA and jerk were highly variable in relation to mouth opening and averaged 1–2 s before that event (Table 1). It is thus unlikely that these peaks indicate mouth opening and closing events; instead the increased jerk and MSA signals are most likely related to fluking action and other body positioning in preparation for the lunge.

Blue whales had maximum speeds approximately 1.5 times higher than those of humpback whales (Table 1), largely in agreement with past studies [1], and had a gape cycle about 2.5 times as long as that of humpbacks feeding on krill, but the overall relationship of engulfment to maximum speed and the shape of the speed profile were similar (Figure 3) and consistent between lunges. Humpbacks feeding on fish exhibited more variable timing of engulfment relative to speed and more variable maneuvering during lunges. Although blue whale lunges can vary with respect to approach mechanics (e.g., straight ahead, lateral, and 180° or 360° rolls) [17, 18], the pre-engulfment phase frequently involves acceleration from below the prey followed by an inversion (i.e., 180°) roll coincident with mouth opening. The blue whales in this study exhibited a flipping behavior (Movie S1) in which they approached prey with a near-vertical (rostrum-up) orientation, began engulfment, flipped ventral-side up (i.e., rolled 180°), and then rolled back to a dorsal-up orientation during filtration, and the kinematics of these maneuvers were consistent across lunges (Figure 3F). Similarly, humpback whales feeding on krill had consistent approach characteristics between lunges but did not exhibit large roll excursions (Figure 3G). In contrast, humpback whales feeding on fish had high variability in lunge approach orientation (Figures 3D–3H) and had approximately twice the cumulative heading changes on approach (95% confidence interval [CI] 1.5 to 2.5 times as much as krill-feeding humpbacks), signaling increased maneuvering in the horizontal plane (Figures 2 and 3D; Movie S2).

Table 1. Timing of Kinematic Events during Blue Whale and Humpback Whale Lunge Feeding

	Peak Speed to Mouth Open (s)	Speed Inflection to Mouth Close (s)	Mouth Open to Mouth Close (s)	Mouth Open to Maximum Gape (s)	Duration of Maximum Gape (s)	MSA Peak to Mouth Open (s)	First Jerk Peak to Mouth Open (s)	Maximum Speed (m/s)	Mean Speed (m/s) during Maximum Gape	Minimum Speed[a] (m/s) during Filtration
Blue Whales (Krill)										
Mean	0.0	0.7	4.9	1.6	1.0	2.0	1.7	3.9	2.9	1.1
SD	1.0	1.1	0.8	0.4	0.9	1.8	2.5	0.8	0.4	0.4
No.	25	24	24	25	24	25	25	25	24	25
Humpback Whales (Krill)										
Mean	0.2	−0.3	2.0	0.7	0.5	1.2	1.3	2.7	2.2	1.0
SD	0.7	0.8	0.5	0.2	0.6	0.9	0.9	0.7	0.3	0.3
No.	16	16	15	16	19	16	16	20	19	20
Humpback Whales (Fish)										
Mean	1.1	0.0	4.8	1.2	2.1	1.2	0.9	2.5	1.9	1.0
SD	2.8	3.3	3.0	0.6	2.9	2.1	2.0	0.4	0.5	0.2
No.	32	31	32	32	32	32	32	32	32	32

All times are in seconds. "No." is the number of lunges. See also Figure S3.

[a]The minimum speed attained within 20 s of mouth opening. Of these measurements, 17 out of 25 blue whale lunges, 17 out of 20 humpback whale lunges on krill, and 31 out of 32 humpback whale lunges on fish had minimum speeds at or below the minimum detectable speed.

Regardless of how much of the engulfment phase overlapped with the acceleration phase, all whales decelerated during a lunge-feeding event. The mean minimum forward speed attained within 20 s of mouth opening is reported in Table 1; however, for 65 of 77 whales this was within the lower bound of detectable speeds (~1 m s^{-1}), implying that the minimum speed could be lower than reported. Observations of feeding blue and humpback whales suggest that they maintain some momentum after engulfment, but the increase in bulk (more than doubling in size [1]) and associated increase in drag contribute to continued deceleration during the filtering phase. Thus, it appears that blue and humpback whales in this study did not completely stop, as proposed in the lunge-stop model associated with the peak speed mouth opening hypothesis [2], but did most likely slow down below the speeds proposed in the maintaining-momentum model that is associated with the early mouth opening hypothesis [7]. The momentum maintained after engulfment may be determined by the size of the engulfed water mass relative to the whale's body mass, a functional characteristic that exhibits positive allometry [1]. Blue whales have greater mass-specific engulfment capacity relative to humpback whales, so the amount of momentum transfer from the whale to the engulfed water may be relatively greater in blue whales; thus, blue whales would predictably conserve less momentum after engulfment than humpback whales [19].

DISCUSSION

Our analyses demonstrate a previously unrecognized level of prey-dependent kinematic diversity during rorqual lunge feeding. Specifically, we show that blue and humpback whales feeding on krill exhibit largely discrete engulfment and body acceleration phases, supporting the peak speed mouth opening hypothesis [5, 6]. However, some fine-scale kinematic differences were evident among krill-feeding whales. For example, the humpback whales that we observed feeding on krill off of South Africa demonstrated a small temporal overlap of body acceleration and engulfment, with mouth opening occurring 0.6 s prior (95% CI 0.4 to 0.9 s prior) to maximum speed. This 0.6 s overlap represents ~25% of the engulfment phase, implying that these whales actively accelerated through the early part of engulfment. Therefore, data from these individuals also support some aspects of the early mouth opening hypothesis [7] that was first postulated from humpback whale data. Although fluctuations in prey density could drive some of the observed kinematic differences [18], all krill-feeding humpback whales opened their mouths much closer to the peak in speed than the 1.8 s temporal overlap predicted by the early mouth opening hypothesis [7].

The kinematic variability measured in fish-feeding humpback whales contrasts with the largely stereotypical profiles that characterize krill feeding (Figure 3). Although many rorqual species feed on both krill and other planktonic prey like forage fish and copepods, blue whales are unique in being mostly obligate krill feeders [20]. In contrast, humpback whales are well known for switching between krill and schooling fish as conditions vary [21]. Krill, though considered plankton, exhibit strong escape responses of up to 50 cm s^{-1} [22] that predators must overcome with fast approach speeds and rapid engulfment behaviors.

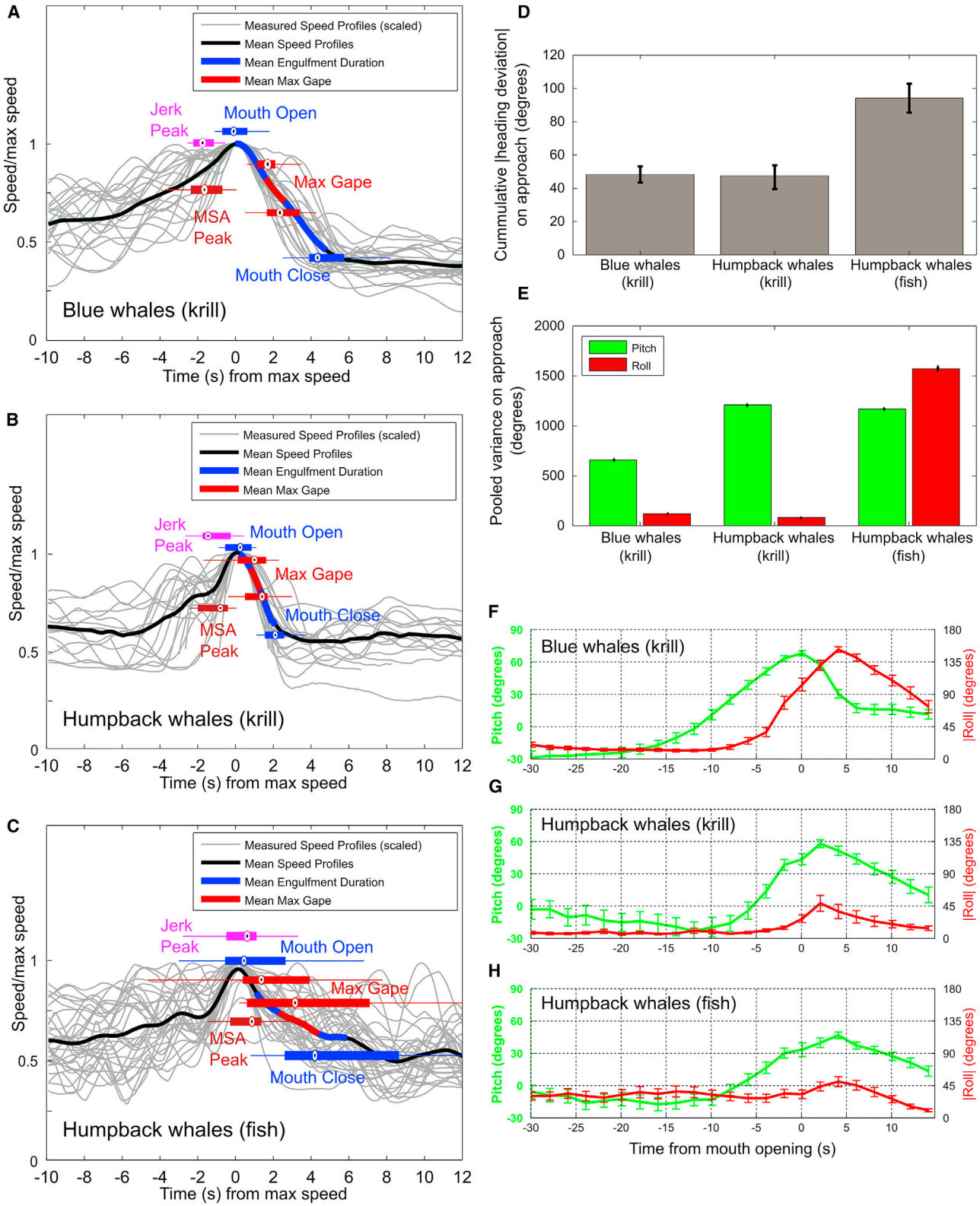

Figure 3. Observed Speed Profiles and Body Orientation during Lunges for Blue Whales Specializing on Krill and Humpback Whales Feeding on Krill or Fish

(A–C) Speed profiles. Thick lines are the mean speed values and a representation of the mean engulfment cycle for each set of lunges. The lengths of box whiskers represent the entire range of data, the central oval indicates the median value, and the edges of the box are the 25th and 75th percentiles.

(legend continued on next page)

Typical humpback ichthyoid prey, however, are even more evasive. Small fish (e.g., 10 cm in total length) have estimated maximum escape speeds ranging from 90 cm s^{-1} (*Engraulus japonicas*) to 2.5 m s^{-1} (*Sprattus sp.*) [23–25]; thus, humpback whales feeding on fish must account for the increased mobility of prey by utilizing more dynamic foraging strategies.

Although blue whales exhibit higher lunge speeds (Table 1) [1], humpback whales have relatively large flippers and flukes that enhance acceleration and maneuverability [26]. In other predators, turning capacity is inversely related to attack speed [27], and this trade-off is evident in the divergent foraging strategies between humpback and blue whales. As obligate krill feeders, blue whales have most likely adopted an optimal strategy for pursuing this specific prey type using extremely large mouths in concert with high-speed lunges to easily overcome krill escape responses [1]. Blue whales maneuver more when targeting lower-density krill patches [17, 18], presumably to access the best available patch in the local environment, yet these maneuvers still follow consistent trajectories (i.e., rolls are largely around the whale's longitudinal body axis) that suggest that the prey are not engaged in escape responses that require extensive pursuit. In contrast, our results demonstrate that humpback whales capture prey using slower lunge speeds, shorter duration gape cycles, and more variable attack angles (Table 1; Figure 3). To fully inflate the buccal cavity with short, low-speed lunges that produce lower stress on the buccal cavity (Table S1), humpback whales exhibit an engulfment apparatus that allows for full inflation with strains that are 75% of those in blue whale buccal cavities [10]. However, this morphology may then limit the ability of humpback whales to lunge at faster speeds when pursuing less agile prey.

An enhanced foraging efficiency has been predicted for blue whales due to their extremely high engulfment capacity [1], and the complex trade-off between maneuverability, lunge speed, and engulfment capacity noted in this study is further indication that humpback whales are less efficient when feeding on krill relative to blue whales. The flexibility of humpback whales as generalist predators to feed on diverse prey, however, may bolster foraging efficiency over broad spatial and temporal scales relative to blue whales.

The ability of different rorqual species to modulate the fine-scale kinematics of the skull and body suggests that high-cost foraging strategies (i.e., increased maneuvering and temporally coupled acceleration-engulfment phases) can be used to capture more agile but possibly higher-quality prey. Alternatively, low-cost foraging methods (i.e., decreased maneuvering and temporally decoupled acceleration-engulfment phases) could be employed by both study species when targeting less agile prey like krill. These trade-offs imply that the prey density thresholds necessary to support these large predators [28] are not solely dependent on differences in body size and energetic requirements, but are also determined in part by the predator's foraging capability and the prey's escape performance. This observation is also supported by fundamental differences in behavior and ecological niche; although blue whales and humpback whales in pursuit of krill are generally solitary feeders, humpback whales feeding on fish may coordinate in groups of two to 15 to employ complex prey-aggregating strategies prior to lunges (e.g., blowing curtains of bubbles [3, 29]). The three western North Atlantic humpback whales in this study foraged on sand lance (~10 cm) that migrated into the water column [30] by producing bubble nets in groups of between one and five animals, whereas whales in Alaska feeding on larger and more mobile herring (~20–30 cm) sometimes feed in groups of up to 15 animals (e.g., [31]). These group behaviors, combined with the ability to modulate the coordination of body acceleration and engulfment timing, allow humpbacks to efficiently exploit different prey types and adapt to dynamic prey conditions in fluctuating climatic regimes [21]. Fin whales (*Balaenoptera physalus*), the second-largest cetacean, exhibit similar morphology to blue whales yet are not limited to krill feeding. Although fin whales are not known to implement complex prey-herding techniques, they have uniquely asymmetrical jaw pigmentation that may aid in corralling mobile prey [32]. Molecular evidence also suggests that fin whales may be more closely related to humpback whales than to blue whales [33, 34]. Fin whales thus represent a key target species for future work in order to refine our understanding of how biomechanical and behavioral processes influence the energetic consequences of predator-prey interactions (Figure S3).

In other aquatic vertebrates that exhibit an integration between locomotion and feeding, behavioral plasticity often reflects broad-scale functional and evolutionary responses to ecological dynamics that force optimization of maneuverability, accuracy, and prey capture speed [35]. The integration of video and movement sensors enables the quantification of locomotion in wild animals and allows for greater estimation of maneuverability parameters and energetic costs. In future work, data from these devices and advanced hydromechanical models should enable more accurate measurements of rorqual lunge-feeding performance and increase our understanding of the ecological role of rorquals as globally distributed apex predators. Rorquals include the largest animals ever and demonstrate both generalist and specialist foraging techniques; continued examination of cetacean predator-prey interactions should shed light on the role of prey specialization in driving predator evolution and foraging success.

(D) Cumulative absolute value of heading changes from 30 to 10 s before mouth opening.
(E) Pooled variance of approach orientation from 30 to 10 s before mouth opening. Error bars indicate the SE of that variation over time as the animal approaches the lunge.
(F–H) Mean pitch and absolute value of roll during lunging by species and prey type.
Error bars in (D) and (F)–(H) indicate the SE. Observe the high degree of stereotypy in the krill-feeding whales, with an acceleration phase always followed by rapid deceleration. Fish-feeding humpbacks show high diversity in feeding strategies, with large data ranges indicating diverse engulfment durations and timings in relation to speed. Although all three types have high orientation changes around the time of mouth opening, humpback whales feeding on fish are unique in having large changes in yaw during approach. See also Figure S3 and Table S1.

SUPPLEMENTAL INFORMATION

Supplemental Information includes Supplemental Experimental Procedures, three figures, one table, and two movies and can be found with this article online at http://dx.doi.org/10.1016/j.cub.2016.07.037.

A video abstract is available at http://dx.doi.org/10.1016/j.cub.2016.07.037#mmc5.

AUTHOR CONTRIBUTIONS

Conceptualization, J.A.G., D.E.C., and A.S.F.; Methodology, J.C., A.S.F., D.E.C., and J.A.G.; Formal Analysis, D.E.C.; Investigation, J.C., A.S.F., D.E.C., and J.A.G.; Writing – Original Draft, D.E.C. and J.A.G.; Writing – Review & Editing, A.S.F.

ACKNOWLEDGMENTS

We graciously thank the field teams led by M'du Seakamela (South African Department of the Environment) and the crew of the *RV FRS Ellen Khuzwayo*; Dave Wiley (Stellwagen Bank National Marine Sanctuary) and the crew of the *RV Auk*; Brandon Southall and the SOCAL BRS project, including the crew of the *RV Truth* (funded under grants from the Navy's Living Marine Resources Program and the Office of Naval Research); and Gustavo Chiang and the crew of the *MV Khronos*. We also thank Silverback Films and The Blue Serengeti Project for financial support; Galatee Films, Silverback Films, and the BBC for providing diver and aerial footage; and Kelly Barr for data preparation. All data collected under National Marine Fisheries Service permits 16111, 15271, and 14809; South African permit RES2015/DEA; Chilean Permit MERI-488-FEB-2015; and individual IACUC protocols. Support for D.E.C. was provided by Stanford University's Anne T. and Robert M. Bass Fellowship and for J.A.G. by the Office of Naval Research's Young Investigator Award.

Received: April 9, 2016
Revised: June 21, 2016
Accepted: July 14, 2016
Published: September 22, 2016

REFERENCES

1. Goldbogen, J.A., Calambokidis, J., Croll, D.A., McKenna, M.F., Oleson, E., Potvin, J., Pyenson, N.D., Schorr, G., Shadwick, R.E., and Tershy, B.R. (2012). Scaling of lunge-feeding performance in rorqual whales: mass-specific energy expenditure increases with body size and progressively limits diving capacity. Funct. Ecol. *26*, 216–226.
2. Goldbogen, J.A., Calambokidis, J., Shadwick, R.E., Oleson, E.M., McDonald, M.A., and Hildebrand, J.A. (2006). Kinematics of foraging dives and lunge-feeding in fin whales. J. Exp. Biol. *209*, 1231–1244.
3. Jurasz, C.M., and Jurasz, V.P. (1979). Feeding modes of the humpback whale (*Megaptera Novaeangliae*) in southeast Alaska. Scientific Reporting of Whales Research Institute *31*, 69–83.
4. Watkins, W.A., and Schevill, W.E. (1979). Aerial observation of feeding behavior in four baleen whales: *Eubalaena glacialis*, *Balaenoptera borealis*, *Megaptera novaeangliae, and Balaenoptera physalus*. J. Mammal. *60*, 155–163.
5. Goldbogen, J.A., Pyenson, N.D., and Shadwick, R.E. (2007). Big gulps require high drag for fin whale lunge feeding. Mar. Ecol. Prog. Ser. *349*, 289–301.
6. Potvin, J., Goldbogen, J.A., and Shadwick, R.E. (2009). Passive versus active engulfment: verdict from trajectory simulations of lunge-feeding fin whales *Balaenoptera physalus*. J. R. Soc. Interface *6*, 1005–1025.
7. Simon, M., Johnson, M., and Madsen, P.T. (2012). Keeping momentum with a mouthful of water: behavior and kinematics of humpback whale lunge feeding. J. Exp. Biol. *215*, 3786–3798.
8. Potvin, J., Goldbogen, J.A., and Shadwick, R.E. (2012). Metabolic expenditures of lunge feeding rorquals across scale: implications for the evolution of filter feeding and the limits to maximum body size. PLoS ONE *7*, e44854.
9. Acevedo-Gutiérrez, A., Croll, D.A., and Tershy, B.R. (2002). High feeding costs limit dive time in the largest whales. J. Exp. Biol. *205*, 1747–1753.
10. Shadwick, R.E., Goldbogen, J.A., Potvin, J., Pyenson, N.D., and Vogl, A.W. (2013). Novel muscle and connective tissue design enables high extensibility and controls engulfment volume in lunge-feeding rorqual whales. J. Exp. Biol. *216*, 2691–2701.
11. Orton, L.S., and Brodie, P.F. (1987). Engulfing mechanics of fin whales. Can. J. Zool. *65*, 2898–2907.
12. Potvin, J., Goldbogen, J.A., and Shadwick, R.E. (2010). Scaling of lunge feeding in rorqual whales: an integrated model of engulfment duration. J. Theor. Biol. *267*, 437–453.
13. Goldbogen, J.A., Calambokidis, J., Oleson, E., Potvin, J., Pyenson, N.D., Schorr, G., and Shadwick, R.E. (2011). Mechanics, hydrodynamics and energetics of blue whale lunge feeding: efficiency dependence on krill density. J. Exp. Biol. *214*, 131–146.
14. Goldbogen, J.A., Calambokidis, J., Croll, D.A., Harvey, J.T., Newton, K.M., Oleson, E.M., Schorr, G., and Shadwick, R.E. (2008). Foraging behavior of humpback whales: kinematic and respiratory patterns suggest a high cost for a lunge. J. Exp. Biol. *211*, 3712–3719.
15. Calambokidis, J., Schorr, G.S., Steiger, G.H., Francis, J., Bakhtiari, M., Marshall, G., Oleson, E.M., Gendron, D., and Robertson, K. (2007). Insights into the underwater diving, feeding, and calling behavior of blue whales from a suction-cup-attached video-imaging tag (CRITTERCAM). Mar. Technol. Soc. J. *41*, 19–29.
16. Owen, K., Dunlop, R.A., Monty, J.P., Chung, D., Noad, M.J., Donnelly, D., Goldizen, A.W., and Mackenzie, T. (2016). Detecting surface-feeding behavior by rorqual whales in accelerometer data. Mar. Mamm. Sci. *32*, 327–348.
17. Goldbogen, J.A., Calambokidis, J., Friedlaender, A.S., Francis, J., DeRuiter, S.L., Stimpert, A.K., Falcone, E., and Southall, B.L. (2013). Underwater acrobatics by the world's largest predator: 360° rolling manoeuvres by lunge-feeding blue whales. Biol. Lett. *9*, 20120986.
18. Goldbogen, J.A., Hazen, E.L., Friedlaender, A.S., Calambokidis, J., DeRuiter, S.L., Stimpert, A.K., and Southall, B.L. (2015). Prey density and distribution drive the three-dimensional foraging strategies of the largest filter feeder. Funct. Ecol. *29*, 951–961.
19. Goldbogen, J.A., Cade, D.E., Calambokidis, J., Friedlaender, A.S., Potvin, J., Segre, P.S., and Werth, A.J. (2017). How baleen whales feed: the biomechanics of engulfment and filtration. Annual Review of Marine Science. http://dx.doi.org/10.1146/annurev-marine-122414-033905.
20. Kawamura, A. (1980). A review of food of balaenopterid whales. Scientific Reports of the Whales Research Institute *32*, 155–197.
21. Fleming, A.H., Clark, C.T., Calambokidis, J., and Barlow, J. (2016). Humpback whale diets respond to variance in ocean climate and ecosystem conditions in the California Current. Glob. Change Biol. *22*, 1214–1224.
22. Kils, U. (1979). Swimming speed and escape capacity of Antarctic krill, Euphausia superba. Meeresforschung *27*, 264–266.
23. Wilson, R.P., Ryan, P.G., James, A., and Wilson, M.-P.T. (1987). Conspicuous coloration may enhance prey capture in some piscivores. Anim. Behav. *35*, 1558–1560.
24. James, A., and Probyn, T. (1989). The relationship between respiration rate, swimming speed and feeding behaviour in the Cape anchovy *Engraulis capensis* Gilchrist. J. Exp. Mar. Biol. Ecol. *131*, 81–100.
25. Wardle, C.S. (1975). Limit of fish swimming speed. Nature *255*, 725–727.
26. Woodward, B.L., Winn, J.P., and Fish, F.E. (2006). Morphological specializations of baleen whales associated with hydrodynamic performance and ecological niche. J. Morphol. *267*, 1284–1294.
27. Wilson, J.W., Mills, M.G., Wilson, R.P., Peters, G., Mills, M.E., Speakman, J.R., Durant, S.M., Bennett, N.C., Marks, N.J., and Scantlebury, M. (2013).

Cheetahs, *Acinonyx jubatus*, balance turn capacity with pace when chasing prey. Biol. Lett. *9*, 20130620.

28. Piatt, J.F., and Methven, D.A. (1992). Threshold foraging behavior of baleen whales. Mar. Ecol. Prog. Ser. *84*, 205–210.

29. Wiley, D., Ware, C., Bocconcelli, A., Cholewiak, D., Friedlaender, A., Thompson, M., and Weinrich, M. (2011). Underwater components of humpback whale bubble-net feeding behavior. Behaviour *148*, 575–602.

30. Hobson, E.S. (1986). Predation on the Pacific sand lance, *Ammodytes hexapterus* (Pisces: Ammodytidae), during the transition between day and night in southeastern Alaska. Copeia *1986*, 223–226.

31. Sharpe, F.A. (2001). Social foraging of the Southeast Alaskan humpback whale, *Megaptera Novaeangliae*. PhD thesis. (Simon Fraser University).

32. Tershy, B.R., and Wiley, D.N. (1992). Asymmetrical pigmentation in the fin whale: a test of two feeding related hypotheses. Mar. Mamm. Sci. *8*, 315–318.

33. McGowen, M.R., Spaulding, M., and Gatesy, J. (2009). Divergence date estimation and a comprehensive molecular tree of extant cetaceans. Mol. Phylogenet. Evol. *53*, 891–906.

34. Steeman, M.E., Hebsgaard, M.B., Fordyce, R.E., Ho, S.Y., Rabosky, D.L., Nielsen, R., Rahbek, C., Glenner, H., Sørensen, M.V., and Willerslev, E. (2009). Radiation of extant cetaceans driven by restructuring of the oceans. Syst. Biol. *58*, 573–585.

35. Higham, T.E. (2007). The integration of locomotion and prey capture in vertebrates: morphology, behavior, and performance. Integr. Comp. Biol. *47*, 82–95.

Current Biology, Volume *26*

Supplemental Information

Kinematic Diversity in Rorqual Whale Feeding Mechanisms

David E. Cade, Ari S. Friedlaender, John Calambokidis, and Jeremy A. Goldbogen

Supplemental Figures

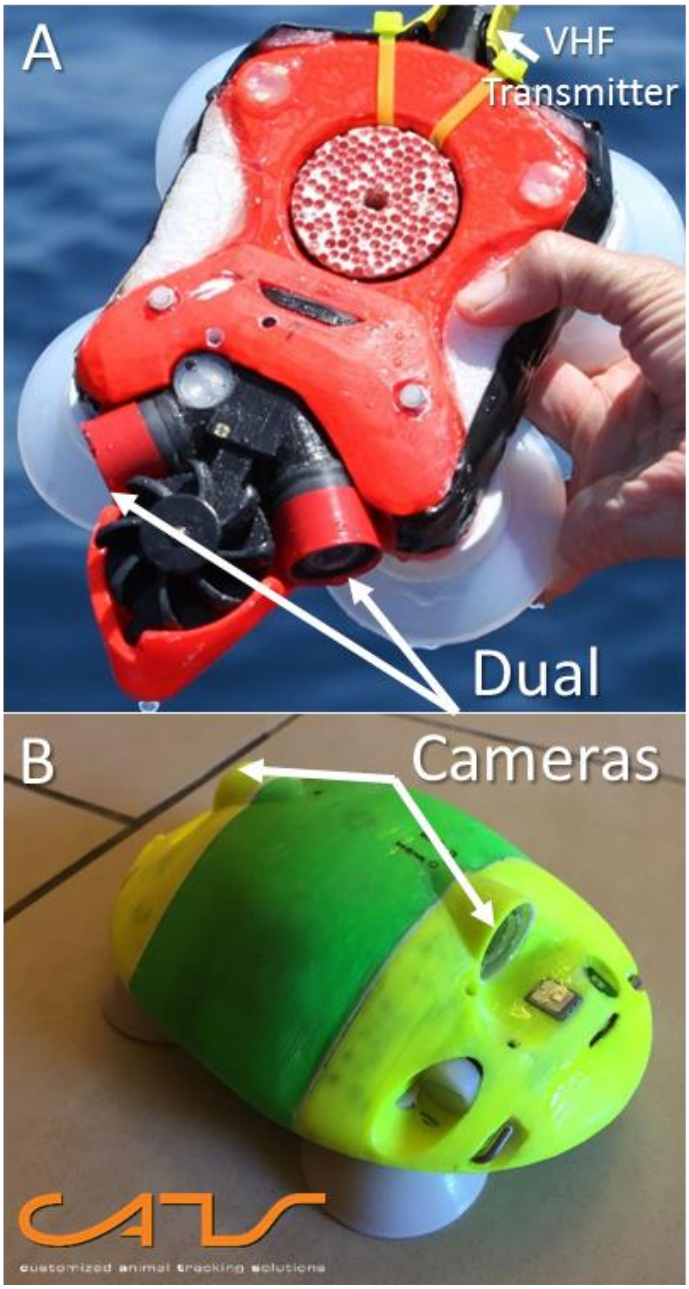

Figure S1- CATS video tags. Related to Figures 1 & 2 and Table S1. A) Initial version p1 tag with 40 Hz accelerometry in a unit that can be separately detached from the flotation. B) Current version m tag with forward and backwards facing cameras, 800 Hz accelerometry, GPS, light, temperature and depth sensors all integrated into the flotation. Both versions adhere with custom-designed suction cups and are recovered via VHF telemetry after floating to the surface. Version p2 (not pictured) used the computer from p1 but with a flotation housing shaped like version m and utilizing DTAG suction cups [S1].

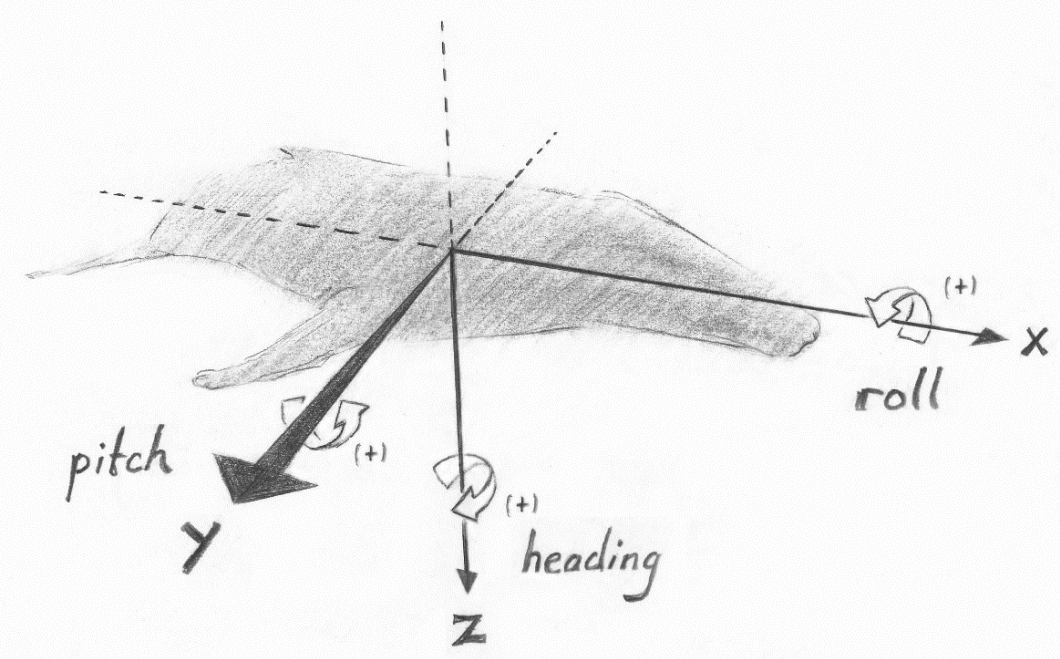

Figure S2- The axis conventions used in CATS video/accelerometry tags. Related to Figures 1 & 2 and Videos S1 & S2. All rotations are positive in the counterclockwise direction when viewed from the positive axis (i.e. *x*: rostral → caudal, *y*: right-side → left-side, *z*: ventral → dorsal). Drawing © Anne Kaferle 2016

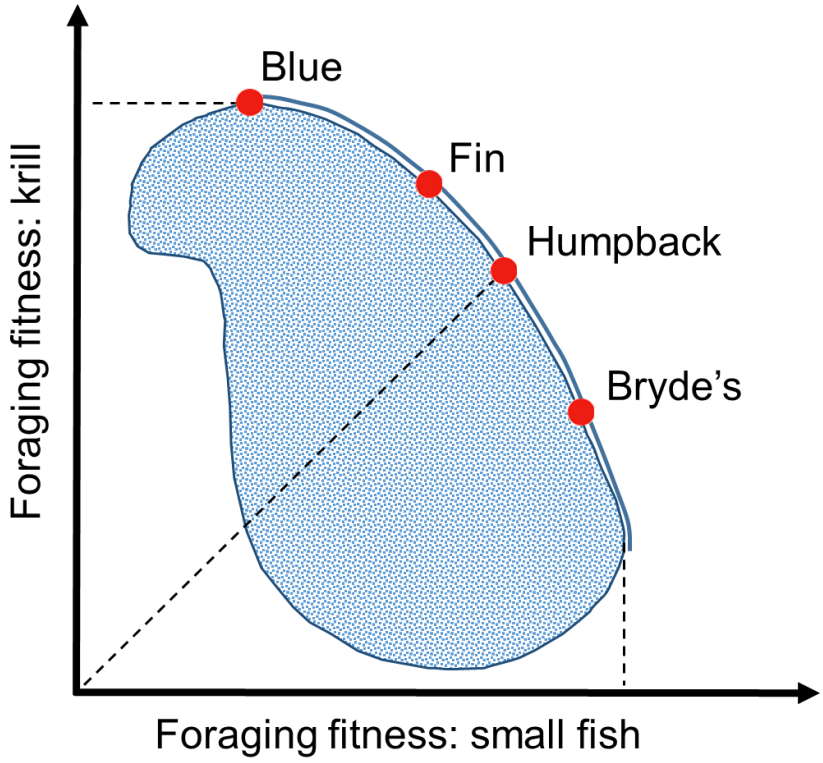

Figure S3- Rorquals as predicted by habitat selection theory [S2]. Related to Figure 3 and Table 1. Balaenopterid species overlain on a foraging fitness set (redrawn from [S2]), with the blue region representing different phenotypes. Different phenotypes have varying success on the two different prey types pictured. Theory predicts that rorquals would occupy the maximally optimized double-lined border of the blue kidney shaped region. As efficiency in one axis increases, fitness in the other decreases. Humpback whales, as a generalist species, would theoretically occupy the space along the dotted line of slope one whereas blue whales, as krill specialists, would theoretically occupy the space in the upper left corner implying they are maximally optimized for feeding on krill. Our work supports this alignment, but further investigation into feeding preferences and optimization is necessary.

Supplemental Tables

Table S1- Morphometric and deployment information for the 14 whales observed in this study. Related to Figures 1-3. Deployment ID includes a species ID (bw = blue whale, mn = humpback whale), date and tag number. Tag version described in the Supplemental Experimental Procedures and shown in Figure S1. FB = front-back, F = front only, P = arranged like tag version p1 (Figure S1A). Measurements listed are means ± standard error. Ventral Groove Blubber (VGB) length calculated from speed and gape cycles (Equation S1), total length calculated allometrically from VGB length (equations S2,S3) [S3], Predicted Maximum Engulfment Capacity calculated from total length, Measured Engulfment calculated from Equation S4, Max VGB Stress described in the text.

Deployment ID	Tag Version	Location	Deployment Length (HH:MM:SS)	Camera Arrangement	Feeding Events (#)	Prey Type	Mean r^2 for Speed-Flow Noise Relationship	Calculated VGB Length	Allometric Total Length	Predicted Maximum Engulfment Capacity	Measured Engulfment	Max VGB Stress
bw140722-2e	p1	Central California	0:49:47	P	1	Krill	0.60	-	-	-	-	
bw140806-2	p1	S. California	3:33:29	P	3	Krill	0.78	15.1 ± 0.3 m	25.7 m	117 m^3	123 ± 4.7 m^3	2020 ± 420 Pa
bw140819-3b	p1	S. California	0:16:36	P	1	Krill	0.61	17.2 m	28.7 m	173 m^3	200 m^3	2550 Pa
bw140820-3b	p1	S. California	1:01:14	P	15	Krill	0.84	12.6 ± 0.4 m	22.1 m	68 m^3	66 ± 2.4 m^3	2030 ± 170 Pa
bw140820-4b	p1	S. California	0:08:05	P	1	Krill	0.74	-	-	-	-	-
bw160224-8	m	Southern Chile	26:00:25	FB	4	Krill	0.39	13.2 ± 0.1 m	23.1 m	80 m^3	90 ± 9.6 m^3	1400 ± 91 Pa
mn150618-4	p2	Stellwagen Bank	7:45:44	P	8	Sand Lance	0.42	-	-	-	-	-
mn150622-2	p2	Stellwagen Bank	6:03:04	P	2	Sand Lance	0.58	-	-	-	-	-
mn150622-4	p2	Stellwagen Bank	14:18:15	P	3	Sand Lance	0.43	-	-	-	-	-
mn151012-7	m	Monterey Bay	5:56:02	FB	19	Anchovy	0.35	5.9 ± 0.5 m	10.5 m	9.8 m^3	9.5 ± 0.7 m^3	1370 ± 180 Pa
mn151031-3	p2	South Africa	2:11:49	P	2	Krill	0.38	6.3 m	11.0 m	11.5 m^3	13.4 m^3	1101 Pa
mn151031-4	p2	South Africa	4:55:13	P	7	Krill	0.63	4.3 ± 0.4 m	8.2 m	3.9 m^3	3.9 ± 0.4 m^3	1480 ± 250 Pa
mn160419-8	m	Monterey Bay	5:40:19	FB	4	Krill	-	-	-	-	-	-
mn160429-37	m	Monterey Bay	10:39:55	F	7	Krill	0.78	4.1 ± 0.3 m	7.9 m	3.4 m^3	3.0 ± 0.2 m^3	2130 ± 260 Pa

Supplemental Experimental Procedures

Tag Specifications & Design

CATS (Customized Animal Tracking Solutions; www.cats.is) camera tags integrate dual video cameras with 800 Hz accelerometers and gyroscopes; 100 Hz magnetometers, pressure and temperature sensors; a 20 Hz internal temperature sensor; and 10 Hz light and GPS sensors. With proper placement with cameras facing towards the mouth, these tags for the first time enable the measurement of gape in wild cetaceans in synchrony with measurements of animal orientation and motion. Videos were recorded in 1280 x 720p HD resolution at between 25 and 30 frames per second, while audio was recorded with a single embedded microphone at a 22.5 kHz sampling rate with 16 bit resolution.

These tags have undergone several iterations in design (Figure S1). Initial versions p1 & p2 used in 2014 were limited to 40 Hz in all sensors, could record video for up to 3.5 hours and did not include GPS. Version p1 (mass: 654 g, dimensions: 23 x 13 x 4.5 cm) employed wide (8.5 cm diameter) suction cups with a mean deployment time on humpbacks and blue whales (overall deployments including those not described in this study) of 1 hour 18 minutes (max: 10 hours 11 minutes). Version p2 (mass: 513 g, dimensions: 19.5 x 13 x 5 cm) housed the initial sensor module in newly designed flotation and suction cups that resulted in improved durability, decreased drag, and improved deployment duration (mean: 5 hours 16 minutes, max: 14 hours 18 minutes). Version m (mass: 571 g, dimensions: 19 x 13 x 5 cm), the current version, with sensors integrated into the flotation, can record up to 8 hours of video, includes redesigned suction cups (diameter 5 cm) and has again improved deployment duration (mean: 15 hours 28 minutes, max: 35 hours). Version p2 (not pictured in Figure S1), is shaped similarly to version m. All tag designs employ replaceable VHF transmitters operating with a lithium ion battery for recovery. Dual cameras have three current arrangements: front & back facing (Figure S1B), a forward arrangement with cameras offset by 90 degrees like version p1 (Figure S1A), and a stereo arrangement with both cameras facing forward with an overlapping field of view (not used in this study). The final deployment (mn160429-37) used a refurbished design with a single camera recording data in 2k video resolution.

Deployment

Tags were deployed from 6 m rigid hull inflatable boats using a 6 m carbon-fiber pole. Tags were attached to the animal with four suction cups, detached after suction failed, floated to the surface and were recovered via VHF telemetry. Deployment lengths in this study ranged from 8 minutes to 26 hours (Table S1). Chilean blue whale tagged under Chilean Permit MERI-488-FEB-2015; all other blue whales tagged under NMFS research permit #16111; US humpbacks tagged under NMFS permit #s 16111, 15271, or 14809; and South African humpbacks were tagged under government permit RES2015/DEA.

Kinematic Analyses from Tag Data

Data from all sensors were downloaded as a standard csv file, imported into MATLAB (Mathworks) and decimated to 10 Hz using a DTAG toolkit script (http://soundtags.st-andrews.ac.uk/dtags/dtag-toolbox/) that employs symmetric finite impulse response filters [S4]. All further analysis described were carried out using custom MATLAB scripts. Videos were recorded in either set time periods of 30 or 50 minutes, or were programmed to turn off when light levels dropped below a set threshold to save battery power. To synchronize video with sensor data, the video frame numbers at which the tag could be seen leaving and entering the water were noted and those points were synchronized with the peaks in the pressure sensor. Calibrations from bench tests were applied to the data and corrections were made for any in situ variations.

Tags reported sensor readings in three axes (tag frame). These values were rotated to match the natural axes of the animal (whale frame) using surfacing events and the first few seconds of dive initiation when the animal could be assumed to be maintaining an upright posture while pitching downwards [S5]. The Euler angles of pitch, roll and heading were calculated at all time points using the accelerometer and magnetometer readings [S1], "jerk" was calculated as the norm of the difference in the accelerometer signals, and minimum specific acceleration (MSA) in units of m s^{-2} was calculated as the absolute value of the norm of the accelerometer signal minus 1 g [S4]. In all versions of these tags, a North-East-Down axis convention was used with pitch, roll and heading counter-clockwise rotations when viewed from the positive direction of the third axis (Figure S2). That is, pitch is positive rostrum up, heading is synonymous with compass bearing from true north, and positive roll is to the animal's right (Figure S2). This rotation convention is in agreement with some prior literature (e.g. [S6]) but in disagreement with others (e.g. [S1]). Gyroscope measurements could be used to correct orientation when Euler angle calculations are known to be

inaccurate during times of high pitch angle (gimbal lock) and when dynamic acceleration was high, but these corrections were not necessary for this study.

Speed Determination

Precisely calculating the speed of cetaceans from tag data has a number of challenges, not least of which is that any point on the body of the animal undulates with fluking motion in a direction perpendicular to forward speed. Currently no consistently accurate, tag-orientation independent forward speed sensors exist for cetacean tags, and researchers commonly use the amplitude of flow noise over tag acoustic devices to estimate speed and to identify high speed events as it has been shown to correlate with increased speed (e.g. [S7-9]). Initial versions of CATS tags attempted to solve this problem with an attached paddle wheel (Figure S1a) that worked well as a speed sensor only occasionally and was subject to stalling at low speeds and to changes in orientation with respect to the flow. It also had the marked disadvantage of needing several turns of the wheel to get a speed estimate, making it inaccurate for determining quick changes. Speed derived from flow noise, though subject to errors associated with prediction from regression and from sources of ambient noise, has been shown to increase the efficacy of animal track reconstruction [S10, S11], and since acoustic sampling is carried out in high resolution it has the advantage of allowing detection at high resolution. A promising new method allows for separating ambient noise from flow noise [S12], but this method requires dual hydrophones and current versions of CATS tags have only a single audio recorder. Despite the limited audio capabilities of the video recorders embedded in CATS tags, they generally give good measurements of flow noise in open ocean environments. An additional advantage of using flow noise to calculate speed is that in situ calibrations allow for any differences from tag to tag and in oceanographic conditions to be accounted for in the calibration curve for each deployment. Since the flow noise/speed relationship is dependent on the position of the audio recorder with respect to the flow, the flow noise to speed relationship was calculated separately for each period of the deployment in which the tag on the animal had a different orientation (due to slipping of the suction cups on the animal).

For all whales except mn160419-8, the speed of tagged animals was estimated for each deployment from a calculated exponential relationship between the amplitude of the flow noise over the embedded microphone and the speed during steeply (>45°) pitched ascents and descents that allowed for an orientation-corrected depth rate (OCDR) to be used as a direct measurement of forward animal speed [S7], and then smoothed with a ½ second running mean filter. Flow noise was calculated as the root mean squared amplitude of the 66-94 Hz frequency band in 1 second sliding bins such that the speed resolution matched the sampling resolution of other data (10 Hz). The minimum correlation coefficient for each animal is listed in Table S1. Audio was non-functional for mn160419-8, so analysis was limited for this deployment to times when OCDR was reliable. For the purposes of this study, even in situations where a lack of sufficiently steep ascents and descents did not allow for regression relationships with high correlation coefficients, flow noise still gave an accurate representation of the timing of acceleration and deceleration so was a valuable and consistent metric. During times when conspecific vocalizations or surface noise potentially interfered with calculations of flow noise, the speed profiles were checked against OCDR profiles to ensure that false peaks were not inadvertently chosen. If peaks in speed could not be confidently picked out, lunges were excluded from analysis. Overall, when speed could be calculated from OCDR [S4], the timing of the peaks in speed were close to those for flow noise: 0.5 ± 0.5 s (mean ± s.d.) in absolute time difference.

Video Analyses

Prey type was generally determined from a combination of video observations during feeding events and surface observations of prey aggregations. For South African deployments, tags were recovered with krill stuck in tag cracks and crevices, simultaneous net tows of nearby regions confirmed high krill densities, fecal samples observed during tag deployment were pink in color, and strong differences in echosounder backscatter between the 200 kHz and 38 kHz transducers at the depth of lunges were in agreement with high krill density.

Archival aerial and diver footage of blue whale and humpback whale lunges videos were analyzed to determine how the timing of the lifting of the upper jaw (the primary indication of mouth opening in tag video) coincided with mouth opening and closing. During each observed lunge, the timing of the initial mouth opening, upper jaw lift, start of maximum gape, end of maximum gape, return of upper jaw to standard position and mouth closing were noted. The distributions of these events were assumed to be normal and means were compared using unpaired t-tests. To maximize information from a limited number of data points, each difficult to obtain, lunges from all tagged animals were treated as independent events and thus animals with the most observed lunges had a greater influence on the mean results. Despite this limitation, clear inferences could still be drawn.

The mouth opening time in relation to the loudness of flow noise for a blue whale in the Gulf of California was described in Calambokidis et al. [S13] from an early on-animal camera deployed in 2001. For the current study,

the original analog media was digitized, flow noise was calculated and the timing of the peak speed determined. Flow noise was not converted to animal speed as measurements of animal orientation and depth were not available for this deployment. In the end, this deployment was excluded from further analysis due to several problems with the data: the camera was designed to rotate with the result that the direction of the microphone with respect to flow noise was not consistent, the recordings had generally poor quality in video and audio compared to today's standards, and a jittery camera made it challenging to precisely distinguish when the mouth began opening. All of these issues led to flow noise profiles with several peaks around the lunge events that varied greatly from the clear peaks of the CATS tags. For these reasons, this deployment was not pooled with CATS deployments that did not have the same issues.

Blue whale lunges were easily identifiable in tag deployment videos as times when the upper jaw lifted and prey passed rapidly by the camera (Video S1, Figure 1). In some viewpoints, the grooved ventral pleats were also visibly expanded. These lunges coincided with peaks in speed, high jerk signals and changes in body orientation including steep pitch angles and rolls of greater than 90° as previously assumed to be characteristic of lunges [S7, S14, S15] but not before confirmed visually. Lunges by krill-feeding humpback whales could likewise be detected easily in both the video and accelerometry signals, but lunges by fish-feeding humpback whales were located primarily through video analysis as the accelerometry signals were not always clear.

The timing of mouth opening was determined as the time when any part of the upper jaw could first be seen rising as part of a lunge (Figure 1, Video S1). We justified the assumption of the synchrony of upper jaw lift and mouth opening by analyzing lateral views of the jaw kinematics of blue and humpback whales from aerial and underwater (non-tag) video. Similar to other mammals [S16], our kinematic analyses from non-tag (diver and aerial) footage indicated that the upper jaw elevation of both blue whales and humpback whales is coincident with mouth opening to within 0.1 ± 0.1 s for blue whales and 0.0 ± 0.0 s for humpbacks, and the jaw returns to normal position coincident with mouth closure (0.0 ± 0.0 s apart).

Maximum gape duration was determined as the time from when the upper jaw ceased its upward motion to when it began to move back towards standard mouth-closed position. Timing of mouth closure was determined as the video frame when the upper jaw could no longer be seen to be falling. Because from some tag placement vantage points the back may obscure some portion of upper jaw lift and lowering, and because the upper jaw returned to standard position ~ 1 s before the lower jaw closed completely in 2 of 17 observed non-tag videos, it is possible that the overall timing of the mouth opening may be slightly longer than we recorded by observed upper jaw lift. However, the effect of this portion of the gape cycle on overall gape dynamics and water influx should be minimal since it represents a slow-moving and small gape aperture portion of engulfment.

For selecting peaks in MSA signals, if multiple peaks existed of comparable height, the peak closest to the mouth opening event was chosen. For jerk signals, which were more likely than MSA signals to have multiple peaks of comparable height, a second peak was chosen close to the mouth closing event (Table 1, Figure 2). All video timings were determined to the nearest video frame.

Morphometric Parameters Calculated from Tag Data

The integration of gape cycle observation in concert with 3D kinematic data, including forward speed estimation, enables more precise calculations of the engulfed water mass during a lunge feeding event. All measurements described here are displayed in Table S1.

The length of the ventral groove blubber (VGB) was estimated assuming that the velocity of the engulfed water mass relative to the whale was the same as the whale's velocity relative to the surrounding medium. Thus, the distance the whale travels during a lunge would be the same distance the engulfed water travels into the whale's buccal cavity, and the VGB length (VGB_L) could be estimated by equation S1

$$\mathrm{VGB_L} = \int_{t_0}^{t_1} V_c \, dt \qquad \text{(S1)}$$

where t_0 and t_1 represent the time of mouth opening and mouth closing, respectively, and V_C represents the velocity of the cetacean. Two assumptions were made to allow this calculation: 1) that water entering the mouth pushes back towards the buccal cavity at the speed of the whale and 2) that each lunge fills the buccal cavity to maximum engulfment. While the first assumption would lead to an upper bound on VGB length, the second assumption could result in under-estimation of length estimates if it were not true. In the absence of clear morphometric data, however, these model estimates give good approximations. It should be understood that since data is digitized and sampled, integrals in all equations involving sampled data were estimated using sums of data sampled at 10 Hz.

From the estimate of VGB_L, the total length (TL) of each tagged animal could be estimated using allometric relationships derived by Goldbogen et al. [S3] from measured specimens.

$$\text{Blue whales: } TL = 3.90 + 1.44 \times VGB_L. \quad \text{(S2)}$$

$$\text{Humpback whales: } TL = 2.21 + 1.40 \times VGB_L. \quad \text{(S3)}$$

The predicted maximum engulfment was then derived directly from allometric estimates of jaw length based on TL and an ellipsoidal estimation of buccal cavity size [S17]. The gape angle (γ) at any time t could be estimated using measured timings of mouth opening and closing (Table 1) and an estimate of maximum gape angle [S18] for a given species. Given the gape angle at time t and an allometric jaw length estimate, the mouth area (A_C) of the whale at any given time could be estimated from equation C.1 in [S19]. The total engulfed water (V_W) at any given time, assuming that all water that the mouth area is exposed to is engulfed at the speed the whale is travelling, could then be simply calculated as:

$$V_W = \int_{t_0}^{t_1} V_c \times A_c \, dt \quad \text{(S4)}$$

To get a comparative estimate of the force applied to the buccal cavity wall, F_{BC}, a number of models have been proposed. For the data in Table S1 we used equation 2.5 in [S20] with the constant value k_{S2} interpolated from Tables 1 and 3 in [S18] using the calculated estimate of whale length, and τ equal to the engulfment duration of each individual lunge, measured directly in concert with kinematic data for the first time in this study. The surface area (SA) of the buccal cavity wall was estimated as the surface areas of two quarter ellipsoids [S21]. The integrals in S5 were calculated using Simpson's rule:

$$\begin{cases} SA = 2\pi c^2 + \frac{2\pi ab}{\sin(\phi)}\left[E(\phi,k)\sin^2(\phi) + F(\phi,k)\cos^2(\phi)\right]\Big/_4 \\ E(\phi,k) = \int_0^{\phi}\sqrt{1-k^2\sin^2 x}\; dx \\ F(\phi,k) = \int_0^{\phi}\frac{dx}{\sqrt{1-k^2\sin^2 x}} \qquad , a \geq b \geq c \\ \phi = \operatorname{acos}\left(\frac{c}{a}\right) \\ k = \frac{a^2(b^2-c^2)}{b^2(a^2-c^2)} \end{cases} \quad \text{(S5)}$$

where a, b and c are the three radii of the ellipsoid. For a whale engulfment model, the anterior and posterior sections of the buccal cavity can be modeled effectively as quarter ellipsoids with a running longitudinally, b dorsal-ventrally, and c along the body's transverse axis [S17]. Note that for different moments in time, a, b and c may switch the axis they represent to maintain the convention in the calculation that $a \geq b \geq c$. For our calculations, we assumed c to be constant as half the width of the head (allometrically determined). A variation on Equation S1 was used to calculate a, the longitudinal length of the extended buccal cavity pouch, at any given time t. For SA_A, the anterior surface area, after a increased beyond the length of the jaw a_A was capped at the jaw length. For SA_P, the posterior surface area, $a_P = 0$ until a increased beyond the length of the jaw. Until that point, SA_P was estimated as the area of the ellipse given by semi-major and semi-minor axes b and c. The dorsal-ventral axis, b, was calculated at any moment from the engulfed water volume using the equation for the volume of an ellipsoid:

$$b = \frac{V_W}{\pi/_3 \times c \times a} \quad \text{(S6)}$$

The final surface area at any given time was then $SA_A + SA_P$. Finding the maximum of F_{BC} / SA gave the final buccal cavity wall stresses displayed in Table S1.

Supplemental References

S1. Johnson, M.P., and Tyack, P.L. (2003). A digital acoustic recording tag for measuring the response of wild marine mammals to sound. IEEE Journal of Oceanic Engineering *28*, 3-12.

S2. Rosenzweig, M.L. (1981). A theory of habitat selection. Ecology *62*, 327-335.

S3. Goldbogen, J.A., Calambokidis, J., Croll, D.A., McKenna, M.F., Oleson, E., Potvin, J., Pyenson, N.D., Schorr, G., Shadwick, R.E., and Tershy, B.R. (2012). Scaling of lunge-feeding performance in rorqual whales: mass-specific energy expenditure increases with body size and progressively limits diving capacity. Functional Ecology *26*, 216-226.

S4. Simon, M., Johnson, M., and Madsen, P.T. (2012). Keeping momentum with a mouthful of water: behavior and kinematics of humpback whale lunge feeding. The Journal of Experimental Biology *215*, 3786-3798.

S5. Zimmer, W.M., Johnson, M.P., D'Amico, A., and Tyack, P.L. (2003). Combining data from a multisensor tag and passive sonar to determine the diving behavior of a sperm whale (*Physeter macrocephalus*). IEEE Journal of Oceanic Engineering *28*, 13-28.

S6. Woodward, B.L., and Winn, J.P. (2006). Apparent lateralized behavior in gray whales feeding off the central British Columbia coast. Marine Mammal Science *22*, 64-73.

S7. Goldbogen, J.A., Calambokidis, J., Shadwick, R.E., Oleson, E.M., McDonald, M.A., and Hildebrand, J.A. (2006). Kinematics of foraging dives and lunge-feeding in fin whales. Journal of Experimental Biology *209*, 1231-1244.

S8. Sivle, L.D., Kvadsheim, P.H., Curé, C., Isojunno, S., Wensveen, P.J., Lam, F.-P.A., Visser, F., Kleivane, L., Tyack, P.L., and Harris, C.M. (2015). Severity of Expert-Identified Behavioural Responses of Humpback Whale, Minke Whale, and Northern Bottlenose Whale to Naval Sonar. Aquatic Mammals *41*, 469.

S9. Simon, M., Johnson, M., Tyack, P., and Madsen, P.T. (2009). Behaviour and kinematics of continuous ram filtration in bowhead whales (*Balaena mysticetus*). Proceedings of the Royal Society of London B: Biological Sciences, rspb20091135.

S10. Wensveen, P.J., Thomas, L., and Miller, P.J. (2015). A path reconstruction method integrating dead-reckoning and position fixes applied to humpback whales. Movement Ecology *3*, 1-16.

S11. Laplanche, C., Marques, T.A., and Thomas, L. (2015). Tracking marine mammals in 3D using electronic tag data. Methods in Ecology and Evolution *6*, 987-996.

S12. von Benda-Beckmann, A.M., Wensveen, P.J., Samara, F.I., Beerens, S.P., and Miller, P.J. (2016). Separating underwater ambient noise from flow noise recorded on stereo acoustic tags attached to marine mammals. Journal of Experimental Biology, jeb. 133116.

S13. Calambokidis, J., Schorr, G.S., Steiger, G.H., Francis, J., Bakhtiari, M., Marshall, G., Oleson, E.M., Gendron, D., and Robertson, K. (2007). Insights into the Underwater Diving, Feeding, and Calling Behavior of Blue Whales from a Suction-Cup-Attached Video-Imaging Tag (CRITTERCAM). Marine Technology Society Journal *41*, 19-29.

S14. Goldbogen, J.A., Calambokidis, J., Friedlaender, A.S., Francis, J., DeRuiter, S.L., Stimpert, A.K., Falcone, E., and Southall, B.L. (2013). Underwater acrobatics by the world's largest predator: 360° rolling manoeuvres by lunge-feeding blue whales. Biology letters *9*, 20120986.

S15. Friedlaender, A., Goldbogen, J., Nowacek, D., Read, A.J., Johnston, D., and Gales, N. (2014). Feeding rates and under-ice foraging strategies of the smallest lunge filter feeder, the Antarctic minke whale (*Balaenoptera bonaerensis*). The Journal of Experimental Biology *217*, 2851-2854.

S16. Koolstra, J., and Van Eijden, T. (2004). Functional significance of the coupling between head and jaw movements. Journal of Biomechanics *37*, 1387-1392.

S17. Goldbogen, J.A., Potvin, J., and Shadwick, R.E. (2010). Skull and buccal cavity allometry increase mass-specific engulfment capacity in fin whales. Proceedings of the Royal Society of London B: Biological Sciences *277*, 861-868.

S18. Potvin, J., Goldbogen, J.A., and Shadwick, R.E. (2012). Metabolic Expenditures of Lunge Feeding Rorquals Across Scale: Implications for the Evolution of Filter Feeding and the Limits to Maximum Body Size. PLoS ONE *7*, e44854.

S19. Potvin, J., Goldbogen, J., and Shadwick, R. (2010). Scaling of lunge feeding in rorqual whales: an integrated model of engulfment duration. Journal of Theoretical Biology *267*, 437-453.

S20. Potvin, J., Goldbogen, J., and Shadwick, R. (2009). Passive versus active engulfment: verdict from trajectory simulations of lunge-feeding fin whales *Balaenoptera physalus*. Journal of the Royal Society Interface *6*, 1005-1025.

S21. Olver, F.W.J., Lozier, D.W., Boisvert, R.F., and Clark, C.W. eds. (2010). NIST Handbook of Mathematical Functions (New York, USA: Cambridge University Press).